NUCLEAR REACTIONS -- THEORY

SHOCK COMPRESSION AND EXPANSION IN CENTRAL COLLISIONS

Paweł Danielewicz

Physics of central symmetric reactions of heavy nuclei, in the beam energy range from few tens of MeV to a couple of GeV per nucleon, is investigated within a transport model with explicit nucleon, deuteron, $A = 3$ cluster, pion, and delta and N^* degrees of freedom[1,2].

The dynamics of the central high-energy reactions can be broken down into several stages. A 400 MeV/nucleon Au + Au system at $b = 0$, for which baryon-density contour-plots are shown in Fig. 1, can serve to illustrate points. Following an initial interpenetration of projectile and target densities, the

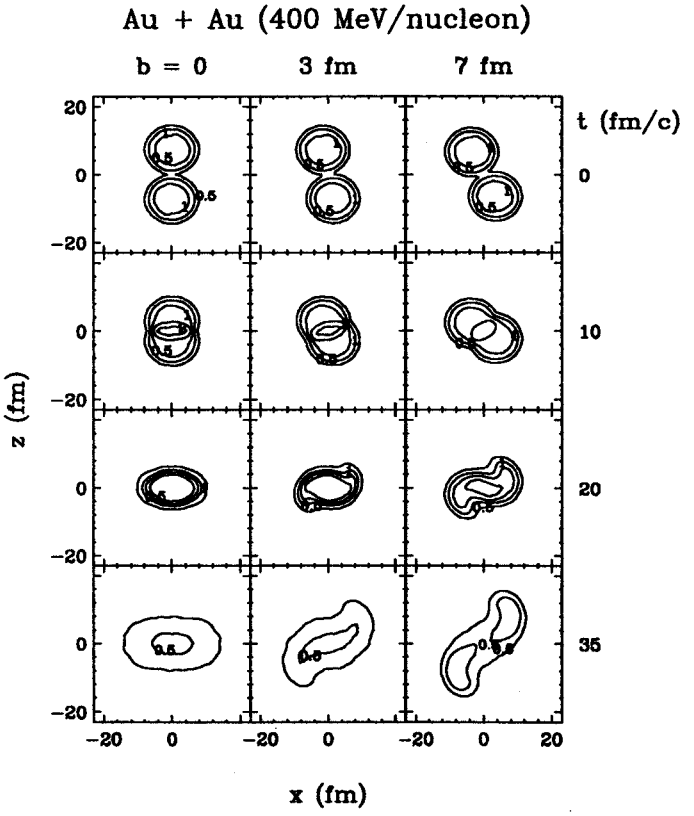

Figure 1: Contour plots of baryon density in the reaction plane in Au + Au collisions at 400 MeV/nucleon from transport-model simulations[2]. The displayed contour lines are for the densities $\rho/\rho_0 = 0.1$, 0.5, 1, 1.5, and 2.

NN collisions begin to thermalize matter in the overlap region making the momentum distribution there centered at zero momentum in the c.m.s. The density in the overlap region rises above normal and a disk of excited and compressed matter forms at the center of the system. More and more matter dives into the region with compressed matter that begins to expand in transverse directions. At late stages, when whole matter is excited, transverse expansion predominates.

If a nuclear system were very large, then it would be necessarily ruled by laws of hydrodynamics. Within hydrodynamics, the initial discontinuity in the velocity field between two nuclei in contact would have to break, at finite times, into two shock fronts travelling in opposite directions into the projectile and target. At low beam energies the shock waves would be weak, not differing much from sound waves. At high energies, the shock waves would be strong leaving behind high density and temperatures. Possibility

of strong-shock formation in head-on reactions was suggested long ago[3]. To assess whether interfaces between normal and compressed matter, such as in Fig. 1, may be interpreted as shock fronts, one can ask whether the state of the matter at the center is such as expected behind a front. The features of the matter behind a developed shock can be determined from the conservation laws of hydrodynamic fluxes, condensed into the Rankine-Hugoniot equation

$$\frac{(e_1+P_1)^2}{\rho_1^2}-\frac{e_0^2}{\rho_0^2}-P_1\left(\frac{e_1+P_1}{\rho_1^2}+\frac{e_0}{\rho_0^2}\right)=0. \tag{1}$$

The parameters with subscripts 0 and 1 refer to the normal and shocked matter, respectively, and e and P are, respectively, the energy density (including mass) and pressure. The energy per nucleon in shocked matter e_1/ρ_1 should be taken equal to the c.m. energy per nucleon. Figure 2 displays baryon density,

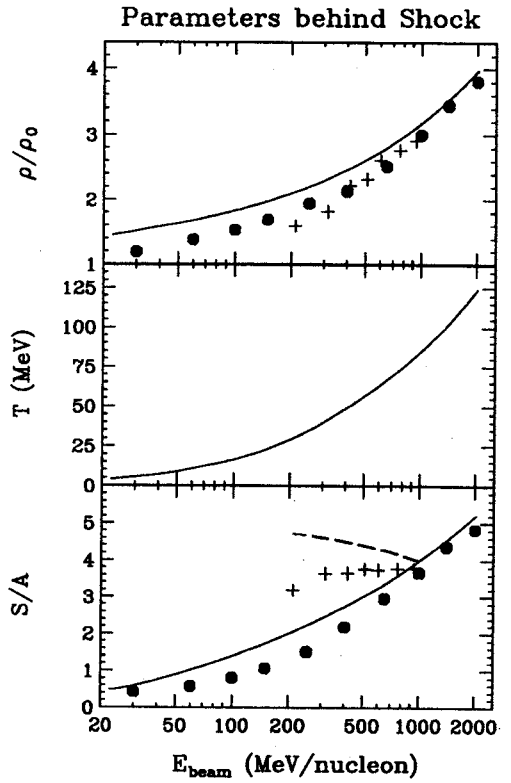

Figure 2: Solid lines show the baryon density (top panel), temperature (center panel), and entropy per baryon (bottom panel) expected behind a developed shock front at $b = 0$, as a function of beam energy, from Eq. (1). Filled circles indicate the maximum density (top panel) and entropy per baryon at maximum density (bottom panel) from the simulations of $b = 0$ Au + Au collisions at different beam energies. Crosses in the top panel indicate the maximum density from the simulations of 1 GeV/nucleon Au + Au collisions at b = 3, 6, 8, 9, 10, 11, and 12 fm, plotted against the beam energy scaled down by a factor equal nonrelativistically to $(1-b^2/4R^2)$, cf. Eq. (3).

temperature, and entropy per baryon from (1), together with a maximum density and entropy per baryon at a maximum density from simulations. The latter follow the general trend predicted by (1). The shocks are nearly completely developed in the high-energy simulations of head-on reactions of heavy nuclei.

Let us now turn to expansion. The hot matter in-between the shocks is exposed in the transverse

directions to vacuum and, as pressure of hot matter is finite and that of vacuum is zero, the matter begins to expand collectively into transverse directions. The features of this process may be understood at a *qualitative* level in terms of the self-similar cylindrically-symmetric hydrodynamic expansion of an ideal gas. In the self-similar expansion, the velocity is proportional to a distance from the symmetry axis, $v = \mathcal{F}(t)\, r$, which roughly holds in the direction of 90° in the $b = 0$ Au + Au collision at 400 MeV/nucleon. Under an assumption of an isentropic flow, the solution to nonrelativistic hydrodynamic equations can be written in terms of the radius R of the matter distribution satisfying

$$\ddot{R}(t) = \frac{2c_s^2}{\gamma R(0)} \left(\frac{R(0)}{R(t)}\right)^{2\gamma-1}, \tag{2}$$

where c_s is initial speed of sound at the origin and γ is heat ratio.

According to (2) the radius should initially increase with a nearly constant acceleration. This is due to the fact that pressure does not change to lowest order with time. At later times, when R is large, the acceleration (2) tends to zero, i.e. R increases linearly with time. This corresponds to a situation where most heat has been converted into energy of collective motion. The drop in acceleration should occur after $t \sim R/c_s$, i.e. the time it takes for a signal to propagate to the center of the system. As radius of gold nucleus is $R \simeq 7$ fm and speed of sound for an ideal gas at 400 MeV/nucleon is $c_s \simeq 0.4c$, this characteristic time for the development of expansion is $R/c_s \sim 20$ fm/c. The dynamics in the direction of 90° in the c.m.s. in the simulation quite closely follows[2] these expectations. In particular, the matter accelerates collectively, e.g. collective transverse energy increases, for about 20 fm/c.

After shocks reach the vacuum along the beam axis, a longitudinal expansion sets in. However, as the transverse expansion is already in progress and decompresses matter, the longitudinal expansion need not acquire same strength. At finite impact parameters, the different starting times for expansion in different directions are responsible for the *squeeze-out*.

The angle α of inclination of the initial plane of discontinuity in velocity relative to beam axis in semicentral reactions is simply given by $\cos\alpha \approx b/2R$. While at $b = 0$ the velocites in both nuclei are normal to the initial plane of discontinuity, the velocities have finite tangential components relative to that plane at a finite b. Such components are continuous across shocks which detach from the initial plane of discontinuity. With tangential components being directed opposite for matter from projectile and target, at the center of the system a so-called tangential discontinuity develops. Density, pressure and entropy are continuous across that discontinuity. Only the tangential velocity component changes. Signs of a weak tangential discontinuity can be seen in Fig. 1 for $b = 3$ and 7 fm at later times. The motion associated with a weak discontinuity, together with the asymmetry in expansion, are responsible for the *sideward deflection* of particles observed in semicentral collisions.

As only the normal velocity component drops to zero across shocks, the shocks are weaker at a finite b than in a head-on reaction. With the normal component being equal to $v_0 \sin\alpha$, the effective c.m. kinetic energy for a shock at a finite b becomes

$$\frac{E_{lab}}{4} \cdot \sin^2\alpha = \frac{E_{lab}}{4}\left(1 - \cos^2\alpha\right) = \frac{E_{lab}}{4}\left(1 - \frac{b^2}{4R^2}\right), \tag{3}$$

rather than $E_{lab}/4$ in the nonrelativistic approximation. In consequence the density behind a shock at a

finite b should be lower than at $b = 0$ and it should, in fact, coincide with the density in a $b = 0$ reaction at beam energy reduced by a factor $(1 - b^2/4R^2)$. That is tested in the upper panel of Fig. 2. In the 1 GeV/nucleon reaction the density appears to follow the expectation up to very high impact parameters.

While certain features of reaction dynamics appear consistent with a hydrodynamic behavior of the matter, there are also important differences. For example, in a system continuing to expanding hydrodynamically temperatures would have dropped to zero and all kinetic energy would get converted into collective energy of expansion. For that collisions would need to continue down to very low densities, which is not the case. For protons emitted in the Au + Au simulations on the average only about 50% of the kinetic energy in the c.m. in the transverse direction is in a collective form, and a higher fraction for heavier particles. The separation of energy into collective and kinetic components is a freeze-out phenomenon.

Generally, the collective expansion affects single-particle spectra. Left panel of Fig. 3 shows momentum distributions of particles emitted from central La + La reactions at 800 MeV/nucleon, in the

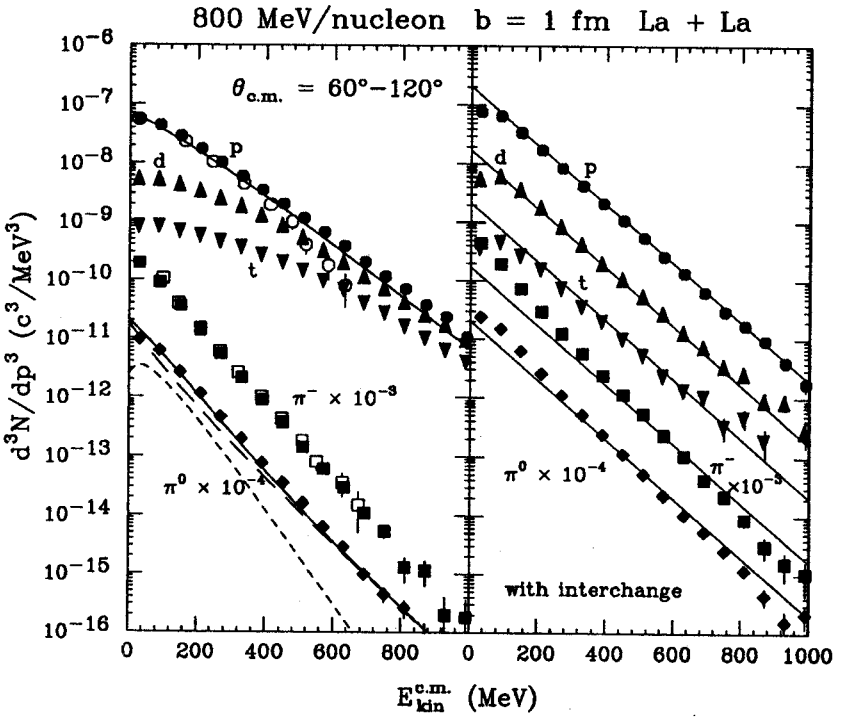

Figure 3: Momentum distribution of protons (circles), deuterons (triangles), helions (inverted triangles), negative (squares) and neutral (diamonds) pions from central 800 MeV/nucleon La + La reaction, in the vicinity of 90° in the c.m. Left panel shows the results of calculations at $b = 1$ fm (filled symbols) and data of Ref. 4 (open symbols). Right panel shows the results of calculations with particle positions interchanged during evolution. Solid lines in the left panel indicate the results of an instantaneous freeze-out model, for protons and neutral pions. Straight parallel lines in the right panel serve to guide the eye.

vicinity of 90° in the c.m. For a large thermalized system, one might expect exponential distributions with same slope corresponding to the temperature inverse. Simulations, though, yield distributions that are increasingly concave down as particle mass increases. The high energy slopes decrease with the increasing mass, corresponding to apparent temperatures of 70, ~ 110, ~ 145, and ~ 175 MeV, for pions, protons, deuterons, and helions, respectively. The slopes increasing with mass and developing concavities are associated with the collective expansion. This is explicitly demonstrated by carrying out simulations

where space-momentum correlations characterizing the collective motion are destroyed by interchanging particle positions when interactions are still frequent, without changing the particle momenta. The emerging momentum distributions are then largely exponential with nearly the same slopes, see Fig. 3.

Changes in the spectra of light fragments with mass in central Au + Au collisions are in a semiquantitative agreement with the data taken at different beam energies by the FOPI Collaboration[5]. The collective energies extracted from dynamics overestimate somewhat those deduced experimentally from intermediate mass fragments[6]. Development of the collective motion strongly affects the production of mesons in heavy collisions, reducing the energy locally available for production, cf. Fig. 4. Missing

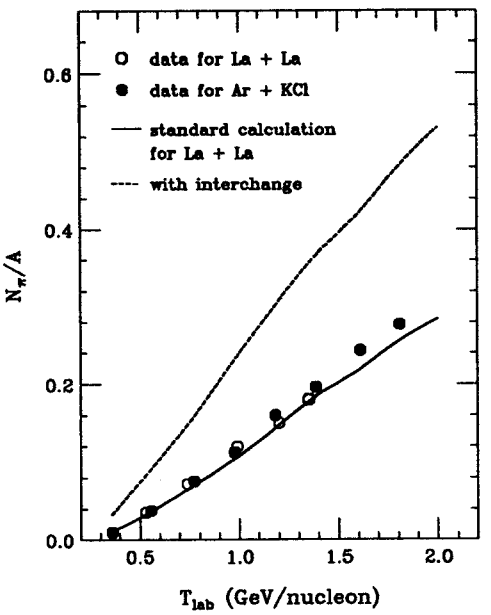

Figure 4: Ratio of the mean pion multiplicity to the number of participant nucleons in central symmetric reactions, as a function of laboratory energy. The solid and dashed lines represent, respectively, the results of standard calculations and of calculations with particle positions interchanged, for the La+La $b = 0$ reactions. The circles represent data of Ref. 7.

energy considered in the past in connection with the pion production [7] may be, at present, identified with the collective energy.

References

1. P. Danielewicz and Q. Pan, in Int. Workshop on Dynamical Features of Nuclei and Finite Fermi Systems, Sitges, X. Viñas, M. Pi, and A. Ramos (eds.), Singapore, World Scientific, 1994, p. 147.
2. P. Danielewicz, Phys. Rev. C51, 716 (1995).
3. G. F. Chapline *et al.*, Phys. Rev. D8, 4302 (1973); W. Scheid *et al.*, Phys. Rev. Lett. 32, 741 (1974); M. I. Sobel *et al.*, Nucl. Phys. A251, 502 (1975).
4. S. Hayashi *et al.*, Phys. Rev. C38, 1229 (1988).
5. FOPI Collaboration and P. Danielewicz, Nucl. Phys. A586, 755 (1995).
6. W. C. Hsi *et al.*, Phys. Rev. Lett. 73, 3367 (1994).
7. W. Harris *et al.*, Phys. Rev. Lett. 58, 463 (1987).

TEMPERATURES OF FRAGMENT KINETIC ENERGY SPECTRA

Wolfgang Bauer

In the study of multifragmentation, the majority of theoretical investigations has been aimed at understanding the fragment mass distributions. However, there is also considerable interest in fragment kinetic energy spectra. In high-energy proton-induced [1] and in relativistic projectile fragmentation [2] reactions one observes Boltzmann-like kinetic energy spectra of intermediate mass fragments with temperatures, for which the fragment mass dependence has been parameterized [1] as $T_f = T_o\,(A_r - A_f)/A_r$, where A_r is the mass of the recoil residue. The temperature T_o typically has a value of $\approx$ 15 MeV, much larger that nuclear temperatures extracted from isotope ratios or level population ratios [3], and also much larger than typical temperatures ($\approx 5-8$ MeV) used in statistical models [4] to reproduced the experimental mass yield curves.

Here we show that the relatively high value of T_f is a consequence of the addition of the Fermi momenta of the individual nucleons in the fragment and thus a consequence of the Fermi-Dirac nature of nucleons. To do this, the single-particle model is employed. It previously was successfully used [5] to explain the observed dispersion in fragment transverse momentum spectra generated in projectile fragmentation.

We start with an ensemble of A nucleons at (internal) temperature T_{in}. In the non-relativistic limit of the single-particle picture their momentum distribution is

$$\rho(\mathbf{p}) = (1 + \exp[(p^2/2m - \mu)/T_{in}])^{-1}\,, \tag{1}$$

where μ is the chemical potential.

When one adds the individual momenta of nucleons in a fragment by sampling from this distribution, then one can calculate the sum momentum from random walk theory. Again in the non-relativistic approximation the kinetic energy of the fragment is $E_f = P_f^2/(2m_N A_f)$, and one arrives at the fragment kinetic energy distribution

$$\rho(E_f) = \frac{2}{\sqrt{\pi\,T_f^3}}\sqrt{E_f}\exp\left(-\frac{E_f}{T_f}\right)\,, \tag{2}$$

where, in this picture, the apparent temperature, T_f, is given by

$$T_f = \sigma^2/m_N = \frac{A - A_f}{A - 1}\,\frac{2}{3}\langle E_k(T_{in})\rangle\,, \tag{3}$$

where $\langle E_k(T_{in})\rangle$ is the average kinetic energy per nucleon at a given internal temperature T_{in}, as obtained from the single particle model. (The factor $\frac{A-A_f}{A-1}$ represent the Goldhaber recoil correction.) The solid curve in figure 1 shows the relation between T_f and T_{in} as obtained from the above relation.

For small temperatures, T_{in}, on can perform a Sommerfeld expansion around $T_{in} = 0$. This yields the approximation

$$T_f(T_{in}) \approx \frac{A - A_f}{A - 1}\,\frac{2}{5}E_F\left(1 + \frac{5\pi^2}{12}\left(\frac{T_{in}}{E_F}\right)^2 + \mathcal{O}\left(\frac{T_{in}}{E_F}\right)^4\right)\,, \tag{4}$$

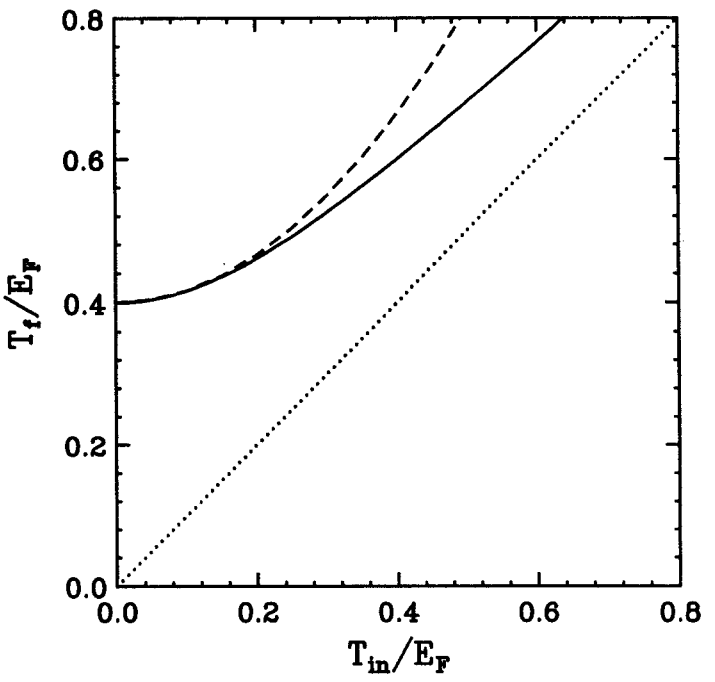

Figure 1: Apparent temperature of fragment kinetic energy spectra, T_f (in units of the Fermi energy), as a function of the internal temperature, T_{in}, of the Fermi gas at breakup. Solid line: result from numerical integration of Eq. 3; Dashed line: analytic approximation, Eq. 4.

which works to better than five percent up to $T_{in}/E_F = 0.3$.

Typical numbers for T_f can be obtained by assuming a freeze-out density of $0.5\,\rho_0$, and a temperature of $T_{in} = 6$ MeV. Then we obtain a Fermi energy of 24 MeV, and a slope constant (ignoring the recoil correction) of $T_f = 12$ MeV. This number is of the order obtained by projectile fragmentation reactions, and it therefore is possible that this kind of fragmentation reactions are not really a cold breakup of nuclei at nuclear matter density (as is conventionally assumed), but the fragmentation of a more dilute system at higher internal temperature. This simple estimate based on the above considerations also shows that it is possible to understand the discrepancy between high fragment kinetic energy temperatures and lower temperatures obtained from level population ratios in one common picture [6].

References

1. R.W. Minich *et al.*, Phys. Lett. B118 (1982) 458; A.S. Hirsch *et al.*, Phys. Rev. C 29 (1984) 508.
2. D.E. Greiner *et al.*, Phys. Rev. Lett. 42 (1975) 152.
3. D.J. Morrissey *et al.*, Ann. Rev. of Nucl. and Part. Sci. 44, 27 (1994).
4. J. Randrup and S.E. Koonin, Nucl. Phys. A356 (1981) 223; J.P. Bondorf, Nucl. Phys. A387 (1982) 25c; D.H.E. Gross *et al.*, Z. Phys. A 309 (1982) 41.
5. H. Feshbach and K. Huang, Phys. Lett. B47 (1973) 300; A.S. Goldhaber, Phys. Lett. B53 (1974) 306; A.S. Goldhaber, Phys. Rev. C 17 (1978) 2243; G.F. Bertsch, Phys. Rev. Lett. 46 (1981) 472.
6. W. Bauer, Phys. Rev. C 51, 803 (1995).

BOSE-ENHANCEMENT AND PAULI-BLOCKING EFFECTS IN TRANSPORT MODELS

W. Bauer and S. Pratt

In heavy-ion collisions quantum statistical effects are important for nucleons at intermediate energy and for pions at high energy. When simulating collisions, extra weights are applied to the collision terms which are proportional to $(1 \pm f)$ for Bose/Fermi particles where f represents the phase-space occupation of particles in the vicinity of the scatterer [1,2]. This problem was originally studied in the context of discreet states in terms of the Einstein A_{nm} and B_{nm} coefficients [3]. The $(1 \pm f)$ prescription is justified given one knows the occupations of the system just before the scattering occurs. However, when measurements are not made between individual scatterings correct treatment of Bose and Fermi statistics requires the incorporation of many-body symmetrization. Our principal objective here is to compare simple models where full n-body symmetrization has been accounted for with the $(1 \pm f)$ method.

If random sources emit distinguishable particles, the probability that n particles will populate a particular state is Poissonian.

$$\begin{aligned} P_0(n) &= \frac{\eta^n}{n!} \exp -\eta \\ \langle n \rangle &= \eta, \end{aligned} \tag{1}$$

where η is the average number of particles emitted into the state. The Possonian distribution assumes there are many trials at emitting the particle and that the product of the number of trials and the probability that a given trial results in emission into the particular state is η.

For the same question with identical particles, one adds a weighting of $n!$ and obtains:

$$\begin{aligned} P(n) &= \eta^n (1 - \eta) \\ \langle n \rangle &= \frac{\eta}{1 - \eta} \end{aligned} \tag{2}$$

Here we have assumed that the quantum matrix element includes a factor of $(a^\dagger)^n$ which contributes an $n!$ enhancement. Such enhancements are valid if the multi-particle emission can be described as one quantum process, meaning that measurements are not made until after emission has halted. The multiplicity distribution is of the Bose-Einstein form, which one can see by replacing η by $\exp -\beta(E - \mu)$.

In semi-classical codes one always assumes that one knows the occupations at all times. Once again, given that η is the number of particles emitted when statistics are neglected.

$$\frac{d\langle n \rangle}{d\eta} = 1 \pm \langle n \rangle, \tag{3}$$

which yields

$$\langle n \rangle = \pm \left(e^{\pm \eta} - 1 \right). \tag{4}$$

The average particle number is shown as a function of η for distinguishable, $n!$-enhanced and $(1 \pm f)$ enhanced emission for both bosons and fermions in Fig. 1. The failure of $(1 \pm f)$ calculations is most noticeable for the Bose case where Bose degeneracy never materializes.

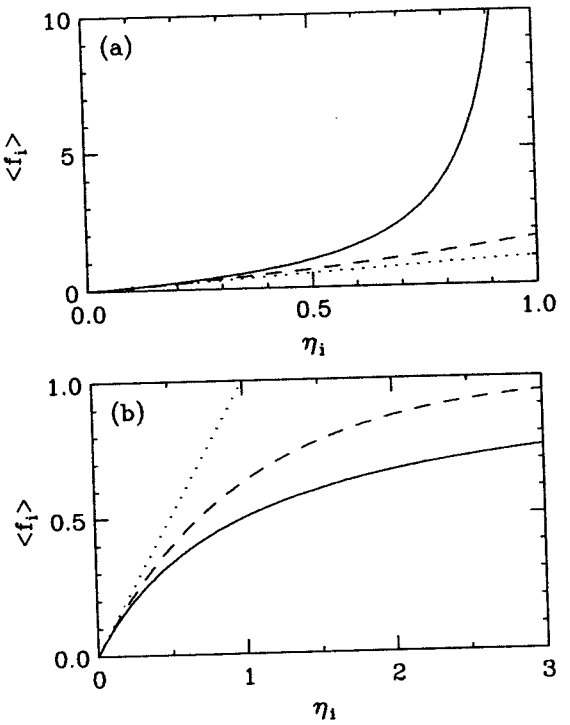

Figure 1: Average population of a Bosonic state as a function of the Poissonian parameter η for the cases of neglected symmetrization (dotted line), $(1+f)$-enhancement (dashed line), and full n-body enhancement (solid line). b: Same comparison for a Fermi gas; $(1-f)$ suppression (dashed line), full n-body suppression (solid line).

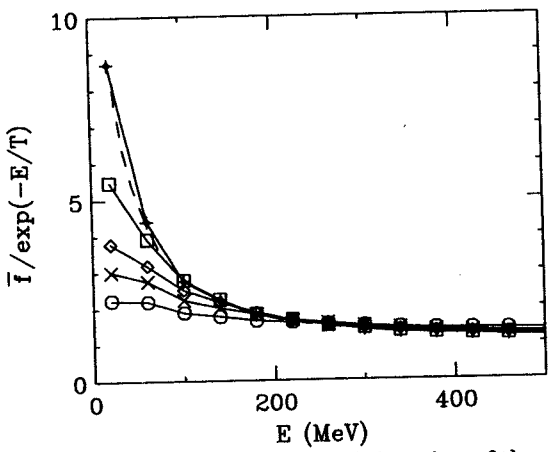

Figure 2: Populations for states, divided by $\exp(-E_i/T)$, as a function of the energy for a system of 200 relativistic particles confined to a 10 fm cube at a temperature of 175 MeV, obtained from $(1+f)$-type simulations and averaged over 10^5 events. Initial populations (circles), after one (crosses), two (diamonds), five (squares), and fifty (upright crosses) collisions per particle. After many collisions populations have approached equilibrium values (dashed line).

Of course, $(1 \pm f)$ calculations will reach equilibrium for a long-lived system where there are many transitions both into and out of all states. To study what period of time is necessary for such equilibrium to be reached we investigate a system of 200 identical pions in a cube 10 fm on a side. Particles are removed randomly and thown back into the system into the eigenstates of the cube with a weight given by the Boltzmann factor multiplied by $(1 \pm n_i)$. Each removal and replacement represents a collision. The temperature was chosen to be 175 MeV. As a function of the number of collisions per particle, Fig. 2 shows the occupation as a function of the energy of the eigenstates. Inspection of Fig. 2 shows that statistical equilibrium was approached after approximately 10 collisions per particle when the maximum occupation is on the order of 10.

For heavy systems, the number of collisions per particle should be near a dozen or more. Thus, for large systems $(1 \pm f)$ theory should be adequate unless Bose degeneracies become larger than 10. However, for small systems, such as those created in $p - p$ collisions, full N-body symmetrization is essential. Reference 4 demonstrates methods for handling N-particle symmetrization for finite systems. Problems discussed here are covered in more detail in Ref. 5.

References

1. G.F. Bertsch, H. Kruse und S. Das Gupta, Phys. Rev. C 29, 673 (1984); H. Kruse, B.V. Jacak, J.J. Molitoris, G.D. Westfall, and H. Stöcker, Phys. Rev. C 31, 1770 (1985); L. Vinet, C. Grégoire, P. Schuck, B. Rémaud, and F. Sébille, Nucl. Phys. A468, 321 (1987); W. Bauer, G.F. Bertsch, W. Cassing, and U. Mosel, Phys. Rev. C 34, 2127 (1986).
2. G. Welke and G.F. Bertsch, Phys. Rev. C 45, 1403 (1992).
3. For a discussion of Einstein's work on stimulated emission see: R.P. Feynman, R.B. Leighton, and M.L. Sands, 'The Feynman Lectures on Physics', Vol. 1, Ch. 42 (Addison Wesley, Reading, 1963).
4. S. Pratt, Phys. Lett. B301, 159 (1993).
5. S. Pratt and W. Bauer, Phys. Lett. B329, 413 (1994).

RADIAL FLOW AND THE BUU TRANSPORT MODEL

F. Daffin, W. Bauer, P. Danielewicz and K. Haglin

Radial flow of protons and light composites from heavy ion reactions has been observed at Lawrence Berkeley Laboratory by the EOS–TPC collaboration[1]. Using Boltzmann-Uehling-Uhlenbeck (BUU) transport model together with a coalescence model we approximate the final state and look for similar effects. BUU has of course been successful in reproducing both the qualitative and quantitative results of experimental studies of directed flow and single-particle correlations. It is natural to ask about the possibility of discerning bulk properties of nuclear matter using radial flow signals. Such properties as the equation of state or medium-modified nucleon-nucleon cross sections would be useful to constrain.

A map of observed radial flows and average temperatures for Au+Au reactions has resulted from the analysis[1] where angular restrictions of 90 $\pm$ 15 degrees in the center of mass were implemented in order to isolate the radial component of the collective expansion. Kinetic energy spectra for protons and light composites were fit to a radially expanding thermal source. Particles possess a thermal velocity distribution within their local rest frame, but carry an additional constant radial velocity component. The resultant distribution is[2]

$$\frac{d^3N}{dp^3} \sim \exp\left(-\gamma E/T\right)\left[\left(\frac{\gamma+T}{E}\right)\frac{\sinh(\alpha)}{\alpha} - \frac{T}{E}\cosh(\alpha)\right], \tag{1}$$

where $\gamma \equiv 1/\sqrt{1-\beta^2}$, $\alpha \equiv \gamma\beta p/T$, T is temperature and $\beta \equiv v/c$ is the flow velocity. After fitting energy spectra to Eq. (1), basically what is seen in the experiment is the following. The temperature seems to rise linearly with beam energy (although errors are large) in the window from 0.25–1.15 GeV while the flow velocity rises—but with some energy dependence that is less clear.

When in the simulation the local density drops below $1/8\rho_0$, we search for nearby particles in both configuration and momentum spaces and with finite probability produce deuterons, tritons, ^{3}He and α particles. The probabilities depend on the coalescence parameters which are adjusted so protons are consistent with the observed spectra. Finally, spectra for the light composites are fit to Eq. (1) from which a flow velocity and common temperature can be extracted. We find flows and temperatures quite consistent with the experimental results of Ref. 1. Sensitivities to details of cross sections, compression and Coulomb effects and others are currently being studied.

References

1. M. A. Lisa *et al.*, "Radial flow in Au+Au collisions at E=0.25–1.15 A GeV", submitted to Phys. Rev. C.
2. P. J. Siemens and J. O. Rasmussen, Phys. Rev. Lett. 42, 880 (1979).

INVESTIGATING MULTIFRAGMENTATION WITH CLASSICAL MOLECULAR DYNAMICS

Scott Pratt, Carlos Montoya and Filip Ronning

For heavy-ion collisions, the emission of fragments is rare at both low energy where evaporative pictures are appropriate and at high energy where coalescence models are justified. At intermediate energy, where the dynamics undergoes a transition from liquid-like to vapor-like behavior, maximum fragment formation occurs [1,2,3].

Given the lack of definitive simulations for Fermi systems at these energies, analyses of fragmentation has relied on simpler models for interpretation. Motivated by the Fisher droplet model, it was predicted that mass distributions would be a power law modified by an exponential:

$$N(A) \propto A^{-\tau} e^{-\sigma A^{2/3} - (\mu_l - \mu_g)A} . \tag{1}$$

For the trajectory that sampled the liquid-gas critical point, the arguments of the exponential would vanish and the mass distribution would be flattest [4]. Fragmentation has also been described with percolation models, where maximum fragmentation would correspond to the bond-breaking parameter being at its critical value. Both critical-phenomena and percolation pictures would predict values of τ near 2.2.

Although classical molecular dynamics is wholly inadequate for describing many aspects of nuclear collisions due to the Fermi degeneracy of nuclear matter, it allows a simple test of the phenomenology. We report on simulations of drops of classical particles which can be condensed, then suddenly heated. By viewing the resulting mass distributions and the microscopic history of the reaction, various scenarios for fragmentation can be tested. This may illuminate the more complex and better hidden mysteries of nuclear collisions. We consider a one-component system with a simple potential that generates a liquid-gas phase transition [5],

$$\begin{aligned} V(r) &= \frac{1}{r^8} - \frac{1}{r^4} - v_0 , \quad r < r_0 \\ &= 0 , \quad r > r_0 , \end{aligned} \tag{2}$$

where $r_0^2 = 10$ and v_0 is chosen such that the potential is continuous. Simulating particles of unit mass with this potential confined to a cubic geometry allows one to determine the critical temperature and density either through the virial theorem, or through examining fluctuations. Both methods point to a critical temperature near 0.6 and a critical density near 0.3.

To investigate fragmentation, N particles were condensed, cooled, then microcanonically excited to an excitation energy, $(3/2)T_0$. Fig. 1 summarizes the mass distributions by displaying τ as a function of T_0 for three different system sizes, N=93, 251 and 485. For each point the resulting mass distribution was fit to a power law, $A^{-\tau}$, for A between 4 and 30. The lowest value of τ corresponds to the flattest mass distribution. For the values of T_0 where τ was minimized the fit to the power-law distribution was excellent for cluster sizes between 4 and 30.

Density-temperature trajectories were calculated by analyzing particles in a small sphere around the origin. Temperatures were obtained by taking two thirds of the average energy per particle. Fig. 2 illustrates trajectories for the N=251 case at three initial temperatures. At the low temperature the system expanded and contracted back towards saturation density, slowly cooling through evaporation. At

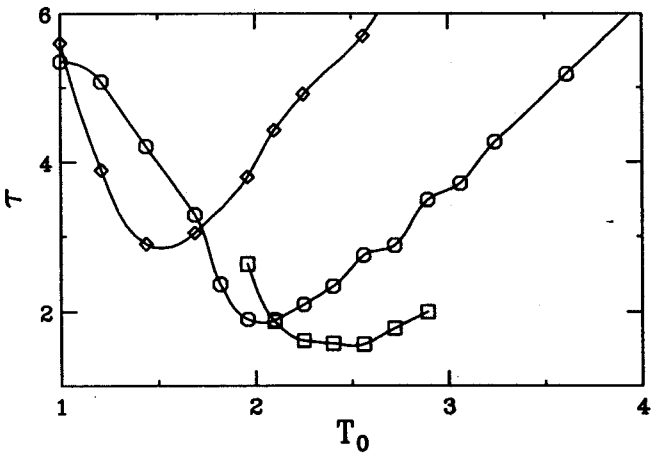

Figure 1: Fitted values of τ as a function of initial temperature for three sizes: 93 particles (diamonds), 251 particles (circles) and 485 particles (squares). For large systems minimum values of τ fall well below 2.0.

the high temperature the drop exploded into small fragments. At the intermediate excitation minimum τ resulted. The density and temperature for this trajectory stalled, as the system neither expanded quickly into a gas nor collapsed back into a liquid drop.

From Fig. 1 one can see that the scaling hypotheses of the critical-behavior and percolation explanations are dubious. For larger systems τ goes well below two, which is inconsistent with scaling since the net fragments number would be unbounded. These values of τ resulted even though the largest fragment was always subtracted from the analysis. One might obtain values of minimum τ near 2.2, but only if the choice of N was fortuitously near 175 parcticles. Furthermore the density-temperature trajectory was far from the critical point for the minimum-τ case. Investigating a confined and equilibrated system at these temperatures and densities results in values of τ near six.

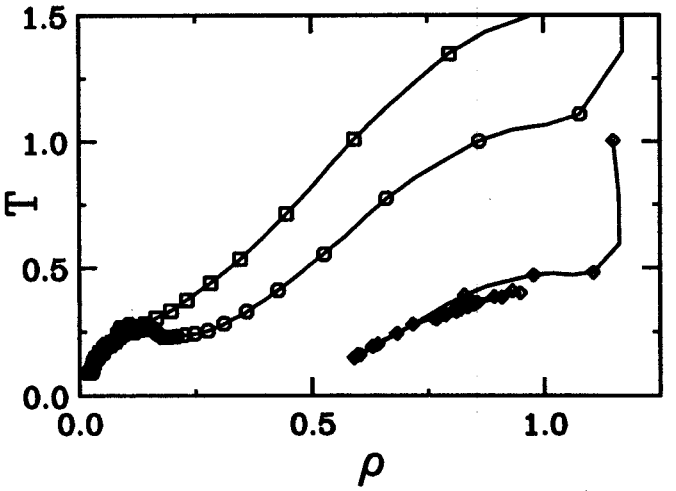

Figure 2: Density-temperatures trajectories of a drop of 251 particles at three different initial excitations. At intermediate exicitation, the reaction balanced between explosion and collapsing back into a drop, and produced the broadest mass distribution.

From our simulations we conclude that the flattest mass distributions resulted from excitations

which led to a dynamical balance between behavior of a liquid and that of a gas. In retrospect this conclusion seems inescapable. At lower excitations, the matter collapses back into a drop and fragmentation must be less by definition, while at higher excitation the fragments are hotter and more likely to dissipate and the expansion stage lasts a shorter time, giving large fluctuations less time to form. This conclusion is at odds not only with scaling pictures but since the conclusions depend crucially on the dynamics, it is also in contradiction with assumptions of chemical equilibration.

References

1. S. Pratt, C. Montoya and F. Ronning, Physics Letters B349, 261 (1995).
2. P.J. Siemens, Nature 305, 410 (83).
3. M.L. Gilkes, et. al. Phys. Rev. Lett. 73, 1590 (94).
4. T. Li, et.al., Phys. Rev. C49, 1630 (94).
5. C. Oglivie, et.al., Phys. Rev. Lett. 67, 1214 (91).

COLLECTIVE STRENGTH IN THE CONTINUUM IN DILEPTON SPECTRA

Vladimir Zelevinsky

The spreading width of a "simple" (single-particle or collective) excitation is due to the mixing with the dense background of complicated states 1. The strength is fragmented over exact stationary states which form fine structure of the spectrum. However the strength function is calculated as a rule as if all states would belong to the discrete spectrum. The finite lifetimes and level widths are governed by the interaction responsible for the decay. This interaction is in general different from that forming the stationary superpositions inside the system. The interplay of these interactions 2 can redistribute strengths and widths and distort significantly the observed pattern.

The approach is developed which allows one to take into account internal and external interaction on equal footing 3. The effective non-hermitian hamiltonian 4, 5 is appropriate for this purpose. This formalism relates the structure of the system to reaction cross sections and by construction guarantees the unitarity of the scattering matrix as well as positiveness of all widths. Let the intrinsic states be $|n\rangle, n = 1, \ldots N,$; let $|0\rangle$ refer to the simple state. N is supposed to be large. The effective hamiltonian of $(N+1) \times (N+1)$ dimension is the operator

$$\mathcal{H} = H - \frac{i}{2}W \tag{1}$$

containing two (real and symmetric for a time reversal invariant system) matrices H and W which describe internal and external coupling respectively. The antihermitian part W is originated by the on-shell decays into open channels $c = 1, 2, \ldots, k$,

$$W = \mathbf{A}\mathbf{A}^T \Rightarrow W_{nn'} = \sum_c A_n^c A_{n'}^c. \tag{2}$$

Here the $(N+1) \times k$ matrices $\mathbf{A} = \{A_n^c\}$ of the real decay amplitudes from intrinsic states $|n\rangle$ to channels c are introduced. The effective hamiltonian $\mathcal{H}$ can be diagonalized to give complex eigenvalues $(j = 0, \ldots, N)$

$$\mathcal{E}_j = E_j - \frac{i}{2}\Gamma_j \tag{3}$$

and the quasistationary eigenstates $|j\rangle$ with pure exponential decay law $\sim \exp(-i\mathcal{E}_j t)$.

Eigenvalues of the intrinsic hamiltonian H are given by the $(N+1)$ roots $E = \epsilon_\alpha$ of the secular equation

$$E - \epsilon_0 - \Sigma_0(E) = 0, \quad \Sigma_0(E) = \sum_n \frac{V_n^2}{E - h_n}. \tag{4}$$

Here the background part h of H (dimension N) is diagonalized first to give the fine structure states with energies h_n. They are coupled to a simple state at energy ϵ_0 by matrix elements V_n. Each eigenfunction $|\alpha\rangle$ of H carries a fraction of the collective strength

$$f^\alpha = \frac{1}{1 + \sum_n V_n^2/(\epsilon_\alpha - h_n)^2}. \tag{5}$$

The smooth strength function can be defined in terms of the average level density of background states $\rho_0(\epsilon)$, or mean level spacing $D = 1/\rho_0$ as

$$P_0(\epsilon) = [f^\alpha \rho_0(\epsilon)]_{\epsilon_\alpha = \epsilon}. \tag{6}$$

It is normalized according to $\int d\epsilon P_0(\epsilon) = 1$.

The solution of eq.(4) requires the knowledge of statistical properties of the background spectrum h_n and matrix elements V_n. Assuming 1 a roughly equidistant dense spectrum of h_n and interaction intensities V_n^2 only slightly fluctuating around their mean value $\langle V^2 \rangle$ at sufficiently strong coupling, $\langle V^2 \rangle > D^2$, the strength function has the Breit-Wigner shape

$$P_0(\epsilon) = \frac{1}{2\pi} \frac{\Gamma^\downarrow}{(\epsilon - \epsilon_0)^2 + (\Gamma^\downarrow)^2/4}. \tag{7}$$

Then the spreading width of the simple state is given by the golden rule,

$$\Gamma^\downarrow \equiv \Gamma_s = 2\pi \frac{\langle V^2 \rangle}{D}. \tag{8}$$

Now we have to take into account the openness of the system. The decay of the background states occurs via evaporation of particles. Due to the intrinsic coupling, the simple state acquires access to the same evaporation channels. Apart from that, a simple state can be open to the direct decay.

The total non-hermitian hamiltonian (1) has $N + 1$ complex eigenvalues (3) which are the roots $z = \mathcal{E}_j$ of the equation (compare to (4))

$$z - \tilde{\epsilon}_0 - \tilde{\Sigma}(z) = 0, \quad \tilde{\Sigma}(z) = \sum_\nu \frac{\tilde{V}_\nu^2}{z - \tilde{\epsilon}_\nu}. \tag{9}$$

Here $|\nu\rangle, \nu = 1, \ldots N$, are the compound states decoupled from the simple mode but coupled to the continuum. The complex energies $\tilde{\epsilon}_0 = \epsilon_0 - (i/2)\gamma_0$ and $\tilde{\epsilon}_\nu = \tilde{h}_\nu - (i/2)\gamma_\nu$ include the direct decay width γ_0 and evaporation widths γ_ν, respectively. Matrix elements $\tilde{V}_\nu = \sum_n V_n \langle n|\nu\rangle$ and real energies $\tilde{h}_\nu$ are renormalized by the coupling through continuum.

In the case of an open system the quasistationary eigenstates $|j\rangle$ can be represented as superpositions of unstable states $|0\rangle, \ldots, |\nu\rangle$. The fraction $\tilde{f}^j$ of the strength of the simple state $|0\rangle$ carried by the quasistationary state $|j\rangle$ is equal, as in eq.(5), to

$$\tilde{f}^j = \frac{1}{1 + L^j}, \quad L^j = \sum_\nu \frac{|\tilde{V}_\nu|^2}{|\mathcal{E}_j - \tilde{\epsilon}_\nu|^2}. \tag{10}$$

When many decay channels of compound states are open, their widths fluctuate very weakly, $\gamma_\nu \approx \gamma_{ev}$. Then one can use (9) to obtain

$$L^j = \frac{\Gamma_j - \gamma_0}{\gamma_{ev} - \Gamma_j}, \quad \text{or} \quad \tilde{f}^j = \frac{\Gamma_j - \gamma_e}{\gamma_0 - \gamma_e}. \tag{11}$$

In other words, the resulting width of the quasistationary state can be found from simple probabilistic arguments,

$$\Gamma_j = \gamma_0 \tilde{f}^j + \gamma_{ev}(1 - \tilde{f}^j). \tag{12}$$

The direct decay width is distributed over all quasistationary states according their fractions of the strength of the original state $|0\rangle$.

The energy dependence of the widths Γ_j is hidden in the equation (9) for complex energies. In the standard model 1 with the equidistant spectrum and constant matrix elements, (9) gives a pair of coupled equations

$$E_j = \epsilon_0 + \frac{1}{2}\tilde{\Gamma}_s \frac{x_j(1-y_j^2)}{1+x_j^2 y_j^2}, \quad \Gamma_j = \gamma_0 - \tilde{\Gamma}_s \frac{(1+x_j^2)y_j}{1+x_j^2 y_j^2}. \tag{13}$$

Here $\tilde{\Gamma}_s$ is the standard spreading width (8) with the matrix elements, and

$$x_j = \cot(\pi \frac{E_j}{D}), \quad y_j = \tanh(\frac{\pi}{2}\frac{\Gamma_j - \gamma_{ev}}{D}). \tag{14}$$

Eqs.(13) can be approximately solved in limiting cases. If the evaporation width γ_{ev} and the resulting widths Γ_j are small, eqs.(13) take the form (12) where the strength function, up to terms $\sim (\gamma_{ev})^3$, is

$$\tilde{f}^j = [1 + (\pi\tilde{\Gamma}_s/2D)(1+x_j^2)]^{-1}. \tag{15}$$

As in (7), one can neglect 1 in the denominator if $\langle V^2\rangle/D^2 > 1$. Then the distribution of quantities y_j and of the decay widths follows approximately the same Breit-Wigner shape (with some corrections).

The cases may exist when the simple state appropriates a high fraction of the collective strength and therefore preserves its individuality. Such states are called the broad poles in the problem of IAS 6. Assuming that the resulting width $\Gamma_0 \equiv \Gamma_{j=0}$ satisfies the condition $(\Gamma_0 - \gamma_{ev}) \gg D$ we have from (14) $y_0 \approx 1$, so that eqs. (13) give for the broad pole

$$E_0 \approx \epsilon_0, \quad \Gamma_0 = \gamma_0 - \tilde{\Gamma}_s = \Gamma^{\uparrow} - \Gamma^{\downarrow}, \tag{16}$$

which is just the definition of the broad pole in 6. The collective strength carried by the broad pole is

$$\tilde{f}^0 = \frac{\gamma_0 - \gamma_{ev} - \tilde{\Gamma}_s}{\gamma_0 - \gamma_{ev}} \tag{17}$$

which differs from unity by an amount proportional to the spreading width $\tilde{\Gamma}_s$. Such a pole disappears when the increasing mixing rate can compete with the direct decay rate, i.e. the spreading width $\tilde{\Gamma}_s$ becomes comparable with γ_0.

This approach will be applied to relate the strength function to the cross sections in various channels and to address the problems of the isospin purity and of disappearance of the collective dipole strength at high excitation energy.

We consider lepton pair production via two-hadron annihilation other than just the pion must be considered.

References

1. A.Bohr and B.Mottelson, *Nuclear Structure*, vol. I, Benjamin, New York, 1969.
2. V.V.Sokolov and V.G.Zelevinsky. Fizika 22 (1990) 303.
3. V.V.Sokolov and V.G.Zelevinsky, *to be published.*
4. C.Mahaux and H.A.Weidenmüller. *Shell-Model Approach to Nuclear Reactions*, North-Holland, Amsterdam, 1969.
5. V.V.Sokolov and V.G.Zelevinsky. Nucl. Phys. A504 (1989) 562.
6. P. von Brentano. Z. Phys. A306 (1982) 63.

PERTURBATIVE QCD IN PARTON CASCADES

J. Murray, G. Kortemeyer, S. Pratt, K. Haglin and W. Bauer

One of the great challenges facing experimental high-energy and nuclear physics during the next decade is determining the nature of the transition from hadronic to quark-gluon degrees of freedom. This transition must exist at sufficient temperature since hadronic degrees of freedom are inappropriate once hadronic densities exceed the normal inverse volume of a hadron, approximately 1.0 fm^{-3}. These conditions should be realized inside the reaction zone of an ultrarelativistic collision of two heavy ions. For this reason the Relativistic Heavy Ion Collider (RHIC), which will collide gold nuclei with energies of 200 $A \cdot GeV$, is under construction at Brookhaven and the LHC at CERN, which will collide heavy ions with energies of 6300 $A \cdot GeV$, has recently been approved.

During the initial stage of a high energy collision, partons represent the appropriate degrees of freedom. With this motivation, parton cascade models have been developed to simulate the initial prethermalized stage of the reaction. A parton cascade [1,2] is a classical description which entails modeling the reaction by creating an ensemble of partons whose motion is governed by relativistic straight line trajectories, punctuated by scattering. These scatterings create off-shell partons, which might then decay or rescatter.

The question we address is whether space-time development can be treated in a classical manner, particularly whether propagation of off-shell partons is either justified or reasonable. Since most partons at mid-rapidity in a high-energy collision are the result of Bremsstrahlung-like diagrams, understanding the space-time coordinates at which they appear is essential to making a meaningful simulation. This importance is amplified by the fact that the incoming nuclei are Lorentz contracted to a few tenths of a fermi, and that the creation times might be additionally enhanced by relativistic γ factors. Thus, the space-time extent which arises from the decay time of partons can easily be greater than the actual longitudinal size of incoming nuclei.

The most common reaction, in a parton cascade, entails two partons colliding to produce three or more partons. In a parton cascade picture this is modeled sequentially, ignoring the interference of various paths. First a collision is chosen which would result in two outgoing partons, both with an effective off-shell mass. The partons would then decay probabilistically, creating an extra parton at each branching. By considering the most simple process, the annihilation of an e^+e^- pair into a virtual photon which decays into three partons, we compare the results for a classical sequential picture such as is used in a parton cascade to results obtained from a correct perturbative treatment which includes all interference effects. Problems associated with the massless nature of most partons and the gauge nature of gluons arise.

To illustrate the problems associated with the massless nature of partons, we consider an elementary Bremsstrahlung process, $\gamma^* \rightarrow q\bar{q}\phi$. We consider the case of radiating a scalar particle rather than a vector particle because it allows us to neglect complications associated with gauge theories. If we allow the scalar particle to only couple to the quark, there is one contributing Feynman diagram. The single Feynman diagram consists of the two possible time orderings depicted below.

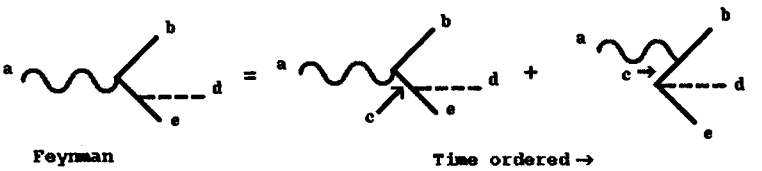

The first process is the actual decay of the virtual photon, with invariant mass Q, into a quark anti-quark pair where the quark later radiates the scalar particle. In the second process, a scalar and a quark anti-quark pair are spontaneously emitted from the vacuum, then the off-shell photon is captured by the anti-quark, leaving all three particles on-shell.

If the cross section is evaluated in the rest frame of the virtual quark, it becomes solely a function of the off-shell mass of the virtual quark and the angle between the quark and anti-quark.

$$\frac{1}{\sigma_0}\frac{d\sigma}{d\cos\theta d\hat{t}} = \frac{\alpha_{\text{scalar}}}{6\pi}\frac{(1-\hat{t})^2 sin^2(\theta/2)}{\hat{t}} \tag{1}$$

By inspecting the Feynman diagram, one might be tempted to interpret Eq. (1) as the probability that a virtual quark, with invariant mass squared $t = \hat{t}/Q^2$, decays into an on-shell quark and scalar. This interpretation is incorrect, because parity conservation demands that the decay of the off-shell quark should be isotropic in its own rest frame.The actual physical interpretation is not clear because the cross section is a consequence of interference between the two different time orderings in Fig. 1. The first time ordering is the actual decay, but the presence of the second time ordering results in the $\cos\theta$ dependence.

If the radiated particle is a gluon, even more severe complications occur. To illustrate this, we consider a process similar to the first, $\gamma^* \to q\bar{q}g$, as in the figure below.

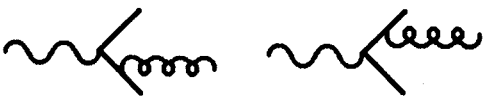

In the leading pole approximation ($\hat{t} \to 0$) and in the limit that the gluon is soft, the cross section, evaluated in an axial gauge defined by the rest frame of the virtual photon, becomes

$$\lim_{\omega\to 0}\frac{1}{\sigma_0}\frac{d\sigma}{d\omega d\cos\theta} = \frac{4\alpha_s}{3\pi}\frac{1}{\omega sin^2\theta} \tag{2}$$

where ω is the energy of the gluon and θ is the angle between the gluon and virtual quark momenta.

The same behaviour can be found in classical radiation from accelerating charges. The energy and angular distribution of radiation from oppositely charged particles moving back to back,

$$\lim_{\omega\to 0}\frac{dN}{d\omega d\cos\theta} = \frac{2e^2\beta^2}{\pi}\frac{1}{\omega sin^2\theta} \tag{3}$$

contains the same pole in the energy spectrum of radiation and angle between the accelerating charge and the observation point. With this insight, the low energy characteristics of the $\gamma^* \to q\bar{q}g$ rate can be attributed to radiation from accelerating the color "charge" of the quark anti-quark pair.

This point is emphasized further by considering the same calculation in an axial gauge defined by the virtual quark's rest frame. In this gauge, only the direct term where the gluon is radiated from the anti-quark has a $sin^2\theta$ divergence; whereas in the previous gauge all of the terms contain a $sin^2\theta$ pole. Both results are consistent with the classical radiation picture. In the rest frame of the virtual quark, only

the anti-quark is accelerated and can radiate color "charge" quanta; whereas the previous gauge was only "physical" in a frame where both the quark and anti-quark were accelerated.

The problems with a cascade come from interpreting Feynman diagrams too literally; the full amplitude for decaying a photon into three particles is more complicated than the simple creation and decay of a virtual quark. The three particle final state is a result of three different scenarios; a virtual parton is created and then decays, a vacuum fluctuation absorbs the photon leaving three on-shell partons, and finally the partons produced by the decaying photon radiate classically. By only considering the contributions from the decay of the virtual parton, more than just 2/3 of the relevant physics is missing. It was shown that the radiated particle was just as likely to be emitted before the photon interacted as after. Neglecting this could have serious consequences, as many pre-equilibrium characteristics are dependent on when and where the mid-rapidity particles are produced. Even more severe implications could occur from ignoring contributions from classical radiation, because it is more than an equal strength effect, it divergently produces low-energy gluons.

One could imagine decaying the off-shell quark according to the full Feynman amplitudes. Such Monte Carlo procedures are standard in the literature and include multiple gluon emission. The $sin^2\theta$-dependence, where θ is the direction of the final state quark as compared to the direction of the anti-quark in the rest frame of the decaying quark, implies that the decaying quark would need to carry information about the anti-quark with which it was created. Such knowledge of its past would require that the time reversed process has knowledge of its future. These considerations would violate the classical nature of the cascade while omitting them would sacrifice detailed balance. Two of the issues one would wish to explore with a simulation is whether the excess of low p_t gluons with respect to low p_t quarks remains after the reaction has proceeded for a long time [3,4], as well as other methods of producing mid-rapidity gluons [5]. Of course when and where the gluons are produced contributes greatly to bulk phenomena such as stopping and chemical potential. Any production mechanism that does not have a space-time component will not effectively model the situation. Until such models include justified space-time prescriptions and formally satisfy detailed balance, conclusions regarding such issues remain dubious.

References

1. K. Geiger and B Müller, Nucl. Phys. A544 (1992), 467c.
2. D.H. Boal, Phys. Rev. C33 (1986), 2206.
3. K. Geiger and B. Müller, Nucl. Phys. B369(1992), 600.
4. P. Carruthers, Phys. Rev. Lett. 50, (1983), 1179.
5. Li Xiong and E. V. Shuryak, Phys. Rev. C49 (1994), 220.
6. R.D. Field, *Applications of Perturbative QCD*, Addison-Wesley Publishing Company, 1989.
7. G. Sterman, *An Introduction to Quantum Field Theory*, Cambridge University Press, (1993), 48.
8. G. Altarelli, G. Parisi, Nucl. Phys. B126 (1977), 298.

CAUSALITY VIOLATIONS IN PARTON CASCADES

G. Kortemeyer, J. Murray, S. Pratt, K. Haglin and W. Bauer

Introduction

Transport models have successfully described many aspects of intermediate energy heavy-ion collision dynamics. As the energies increase in these models to the ultrarelativistic regime, Lorentz covariance and causality are not strictly respected. The standard argument is that such effects are not important to final results; but they have not been seriously considered at high energies. We study how and why these happen, how serious of a problem they may be, and suggest ways of reducing or eliminating the undesirable effects [1].

Causality Violating Mechanisms

Scattering processes in the framework of transport theory are assumed to be non-retarded which, on a microscopic level, leads to information transport with velocities that can approach $\sqrt{\frac{\sigma}{\pi}}/\Delta t_{\text{step}}$, where σ is the parton-parton cross section. As $t_{\text{step}} \rightarrow 0$, it thus can increase without reasonable bound. On a macroscopic level, a series of subsequent causality violating interactions can lead to shock-waves propagating faster than the speed of light in transverse (perpendicular to the beam) direction. This is clearly unphysical.

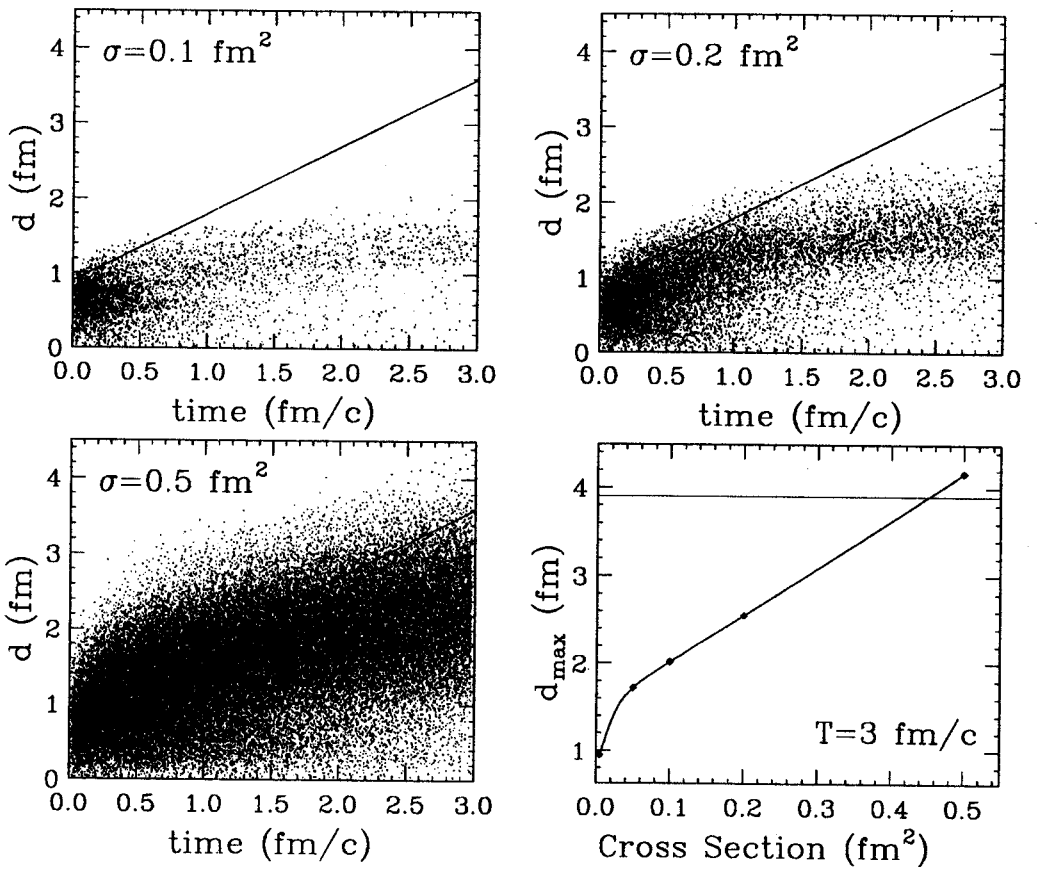

To demonstrate those causality violating shock-waves, the simulation of a (p,Au)-collision was run

with different constant (non-energy dependent) cross sections and S-wave scattering. The figure shows the distance of scattering events from the beam axis versus the simulation time for different cross sections. The solid lines indicate a distance that can only be reached with the speed of light. While during the initial stages of the collisions the outmost scattering events occur at distances larger than those allowed by causality arguments, the information transport soon appears to be damped. It turns out that this phenomenon is not – as one would expect – mainly due to a dropping of the collision rate, but rather to a form of random-walk: only a fraction of the individual signal propagations lead outwards, others have the opposite effect, which results in an effective damping. In fact it turns out that the expectation value of the distance of scattering events from the beam axis is roughly proportional to the square-root of the simulation time, which is a characteristic feature of random-walk mechanisms (compare the top panels of the figure). This mechanism is a valid description until the cross sections are so large that the parton distribution basically appears solid, in that limit the information travels outwards proportional to the simulation time, see the panel for $\sigma = 0.5$ fm^2. Overall for σ=0.2 fm^2 the causality violations are still rather moderate, for 0.5 fm^2 the effect becomes dominant.

The figure also shows the maximum distance of scattering events from the beam axis as they occurred for different cross sections. As it turns out, this value depends linearly on the cross section for an extended range, beyond $\sigma \approx 0.4$ fm^2 the outmost scattering events occur at a distance that can only be reached with superluminous signal velocities.

Mechanisms to Reduce Causality Violating Effects

In many existing cascade codes first steps for dealing with the problem of superluminous signals have been taken: Most of the codes, including ours, allow only one interaction per particle per timestep, a restriction that prevents signals from avalanching over huge volumes within only one timestep. A second restriction implemented in many codes is that in addition to "spatial distance within total cross section" as a criterion for scattering, also the two particles must have reached their point of closest approach assuming their current trajectories [2,3]. This restriction prevents causality violating signal transport in the longitudinal (parallel to the beam) direction, but unfortunately has no effect on the transverse direction. In addition to that, we compare several different other schemes: Methods include simply blocking collisions that would lead to a superluminous signal transport from one collision to the next, artificially introducing a time-delay of the interactions, scaling the cross sections downward while increasing the number of particles, and suppressing low-energy collisions.

Conclusions

The influence of superluminous signal velocities on the signal propagation was found to be smaller than expected. This is mainly due to two effects: In the initial stages of the interaction the energy-dependent cross sections tend to be small. Without this beneficial effect the signal propagation has a threshold in the region between 0.4 and 0.5 fm^2 from where on the velocity of the outgoing shock-wave reaches the speed of light. In the later stages of the interaction shock-waves get damped out because of a signal propagation that resembles a random walk.

References

1. G. Kortemeyer, J. Murray, S. Pratt, K. Haglin and W. Bauer, Phys. Rev. C submitted
2. H. Sorge, H. Stöcker and W. Greiner, Nucl. Phys. A498, 567c (1989)
3. K. Geiger, Phys. Rev. C49, 3234 (1994)

PHOTONS FROM AXIAL-VECTOR RADIATIVE DECAY IN A HADRON GAS

Kevin Haglin

Strange and non-strange axial-vector meson radiative decays contribute to photon production in a hadron gas. One- and two-hadron radiative decay modes of $b_1(1235)$, $a_1(1260)$ and $K_1(1270)$ are studied[1]. At 200 MeV temperature and for a narrow range in photon energies they contribute more to the net thermal photon production rate than $\pi\rho \to \pi\gamma$, $\pi\pi \to \rho\gamma$ or $\rho \to \pi\pi\gamma$. They provide significant contribution to the rate for photon energies as high as 1.5–2.0 GeV, while for higher energies they are less important.

The rate for photon production from a thermalized hadronic system at temperature T whose size is small relative to the photon mean free path is proportional to the imaginary part of the retarded photon self-energy [2,3,4]. For temperatures $100 < T$ the largest contributions to the self-energy will be one- and two-loop diagrams consisting of π's and ρ's. Near T_c, where crossover to a plasma phase is expected, contributions to the self-energy from diagrams in which heavier non-strange and strange particles occupy the loops also become important. If the imaginary part of any of these diagrams (obtained by cutting them) gives a calculated width in vacuum that is relatively sizeable, then even being less abundant than pions or rho mesons in the hot system, it is interesting to ask about their contributions to photon production. Cutting a generic one-loop diagram results in single-hadron radiative decays applied here to either $a_1 \to \pi\gamma$ or $K_1 \to K\gamma$ (since the b_1 decay rate is small). Upon cutting diagrams for two-loop contributions to the b_1, two possibilities arise for the photon being in the final state. First, there could be $\pi b_1 \to \omega \to \pi^0\gamma$ scattering. Secondly, a two-pion radiative decay $b_1 \to \omega\pi \to \pi\pi^0\gamma$ can proceed. The production rate from the first process turns out to be rather unimportant as compared with the second.

Given some radiative hadronic decay channel, the thermal rate is

$$E_\gamma \frac{dR}{d^3p_\gamma} = \mathcal{N}\int \frac{d^3p_a}{(2\pi)^3 2E_a} f(E_a)|\mathcal{M}|^2(2\pi)^4\delta^4(p_a - p_1 - \ldots - p_n - p_\gamma)$$

$$\times \left\{\prod_{i=1}^{n} \frac{d^3p_i}{(2\pi)^3 2E_i}[1 \pm f(E_i)]\right\} \frac{1}{(2\pi)^3 2}. \qquad (1)$$

where $\mathcal{N}$ is the degeneracy and $f(E)$ is either a Bose-Einstein or Fermi-Dirac distribution depending on the species. Bose enhancement(Pauli suppression) is enforced by choosing the $+(-)$ sign in the square-bracketed term. Identifying the species of hadrons and their interactions with other hadrons into which they might decay, and specifying their interactions with the electromagnetic field allows one to write the invariant amplitude $\mathcal{M}$ which then completely defines the problem. What remains is to carry out the necessary four-vector algebra and phase space integration. Details for the model Lagrangians, calibration of coupling constants and vector dominance extrapolations can be found in Ref.[1]

The hadron-gas environment is quite different from free space and induces a thermal broadening to the constituents. It is especially important for the ω in the decay $b_1 \to \pi\omega \to \pi\pi^0\gamma$. While the vacuum width of the ω corresponds to a lifetime of 23 fm/c, the mean free path is at most a few fermis since it can

scatter with pions to form a b_1 resonance[5]. A collisional broadened width

$$\Gamma_\omega^{\rm coll}(E_\omega) = \int ds \frac{d^3p_\pi}{(2\pi)^3} f(E_\pi)\sigma_{\pi\omega}(s)v_{rel}\delta\left(s-(p_\pi+p_\omega)^2\right) \tag{2}$$

is computed, where

$$v_{rel} = \frac{\sqrt{(p_\pi\cdot p_\omega)^2 - 4m_\pi^2 m_\omega^2}}{E_\pi E_\omega} \quad \text{and} \quad \sigma_{\pi\omega}(\sqrt{s}) = \frac{\pi}{k^2}\frac{\Gamma^2_{b_1\to\pi\omega}}{(\sqrt{s}-m_{b_1})^2+\Gamma^2_{b_1}/4} \tag{3}$$

are used with k being the center-of-mass momentum and the full and partial widths are taken to be 155 MeV.

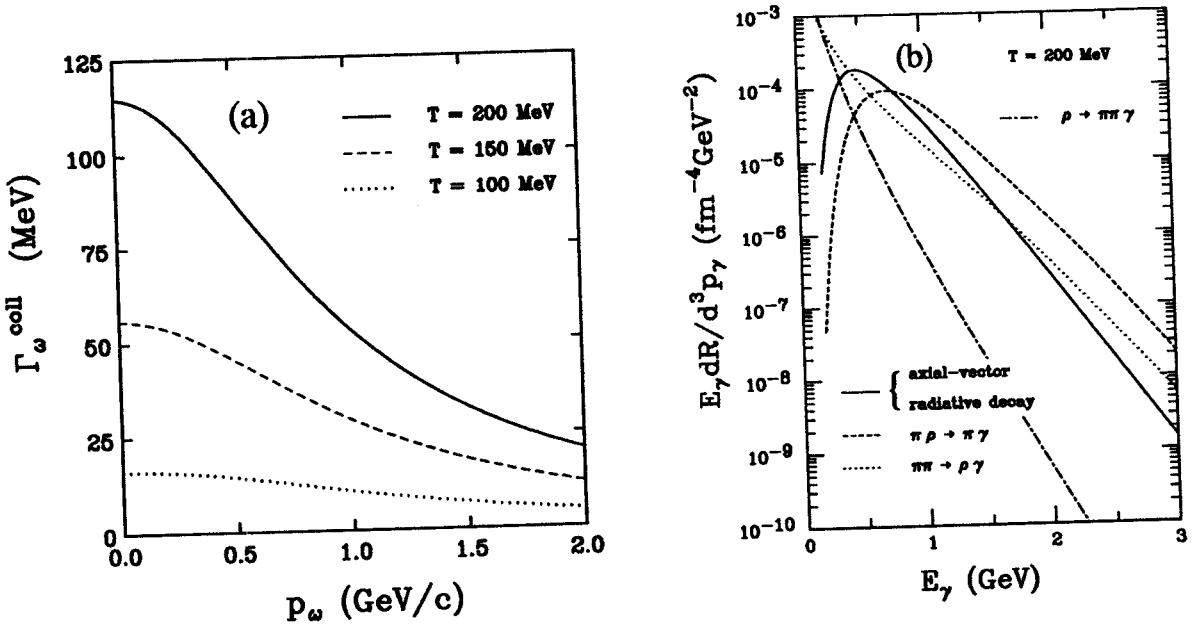

Fig. 1: Collisional broadening of the ω owing to scattering off pions as a function of the ω momentum for three different temperatures (a), and thermal photon production rate (b) from the sum of three axial-vector decays (solid curve) as computed with $\pi\rho \to \pi\gamma$ (dashed curve), $\pi\pi \to \rho\gamma$ (dotted curve) and $\rho \to \pi\pi\gamma$ (dot-dashed curve) at $T = 200$ MeV.

The collision rate for ω is presented in Fig. 1a for 100, 150 and 200 MeV temperature. It is now added to the vacuum width resulting in an energy-dependent full width of

$$\Gamma_\omega^{\rm full}(E_\omega) = \Gamma_\omega^{\rm vac} + \Gamma_\omega^{\rm coll}(E_\omega). \tag{4}$$

Results of carrying out the necessary mathematical steps to arrive at the rates in Eq. 1 for $a_1 \to \pi\gamma$, $b_1 \to \pi\pi^0\gamma$ and $K_1 \to K\gamma$ are shown (summed) in Fig. 1b. Comparison is made at temperature $T = 200$ MeV with the dominant hadronic scattering contributions $\pi\rho \to \pi\gamma$ and $\pi\pi \to \rho\gamma$ as well as the decay $\rho \to \pi\pi\gamma$ taken from Ref. [6,7]. The b_1 results include a collisional broadened omega. Radiative decays contribute more than scattering for photon energies 0.4–0.75 GeV. Then for more energetic photons they

are less important. If one is merely concerned with the overall order of magnitude of the photon energy spectrum, these are clearly not so important. However, at some level in more detailed analyses of the energy spectrum, these axial-vector radiative decays do become important.

Mechanisms for photon production in hot hadronic matter are numerous. Most of them involve species whose abundances are too low or whose scattering rates or decay rates are too small to compete with pion and rho meson processes. There are some with abundances and relevant rates that do in fact compete for limited range in photon energies. Namely, radiative decay of the heavier axial-vector mesons a_1, b_1 and K_1 are relatively important. Contributions from $a_1 \to \pi\gamma$ and $K_1 \to K\gamma$ are comparable to $\omega \to \pi^0\gamma$ with similar photon energy dependence. Contribution of $b_1 \to \pi\pi^0\gamma$ is as large as $\pi\rho \to \pi\gamma$ near its peak which occurs at photon energy 0.5 GeV. However, for photon energies 0.4 GeV and less, other processes like $\pi\pi \to \rho\gamma$ and $\rho \to \pi\pi\gamma$ become dominant. Other heavy mesons do not contribute as strongly as the three axial-vector radiative decays mentioned above. The $\pi\rho$ and $K\rho$ decay channels of a_1 and K_1 are very strong which result in rather large coupling constants. By vector-meson dominance, the electromagnetic-decay coupling constants are also relatively large. Similar remarks can be made about the b_1, but in addition it is also exceptional since one of its most likely decay products is ω. The ω's electromagnetic decay rate is rather large—a partial width of 0.7 MeV. Other non-strange and strange heavy mesons which decay to omega do so with much smaller rates and furthermore, will not be nearly so abundant at temperatures 100–200 MeV.

References

1. K. Haglin, Phys. Rev. C 50, 1688 (1994).
2. H. A. Weldon, Phys. Rev. D 28, 2007 (1983).
3. L. D. McLerran and T. Toimela, Phys. Rev. D 31, 545 (1985).
4. C. Gale and J. Kapusta, Nucl. Phys. B357, 65 (1991).
5. The formalism developed in Phys. Lett. B328, 255 (1994) applied to $\pi\omega$ scattering through the b_1 gives a mean free path for ω of $\bar{\lambda}_\omega$ = 3.5, 1.2 and 0.7 fermis at T = 100, 150 and 200 MeV, respectively.
6. J. Kapusta, P. Lichard and D. Seibert, Phys. Rev. D 44, 2774 (1991); Phys. Rev. D 47, E4171 (1993).
7. C. Song, Phys. Rev. C 47, 2861 (1993).

HIGHER EXCITATIONS OF ω AND ϕ IN DILEPTON SPECTRA

Kevin Haglin and Charles Gale[a]

We consider lepton pair production via two-hadron annihilation through various isoscalar vector mesons within hot, baryon-free matter[5]. This is tantamount to constructing effective form factors which we model using a vector-meson-dominance approach and compare with experiment. In particular, we consider the reactions $\pi\rho \to e^+e^-$ and $\bar{K}K^*(892)$ + c.c.$\to e^+e^-$. We find that $\omega(1390)$ and $\phi(1680)$ are visible in the mass spectrum for the thermal production rate above the $\pi^+\pi^- \to e^+e^-$ tail and even above the $\pi a_1 \to e^+e^-$ results—both of which were considered dominant in their respective mass regions.

After the initial stage of a high-energy heavy-ion collision of the type we consider, which may well include a prehadronic or quark-gluon-plasma (QGP) phase, hadronization gives rise to a hot ensemble of low-lying mesons. Within the context of a thermodynamic model this system's composition has recently been studied[2]. The most abundant hadronic species in this scenario are pions, kaons, ρ-mesons and $K^*(892)$ strange vector mesons owing to the large spin-isospin degeneracy of the last two. With temperatures ranging from phase boundary or crossover temperature downward toward the pion mass or lower, where the system ceases interacting, the number densities of these species range from several hundredths to a few tenths per fm^3[2].

Species can be classified according to their quantum numbers in order to identify the manner with which we model their interactions. Let (P) and (V) represent pseudoscalar and vector mesons. Their interactions are modelled by the Lagrangians[3]

$$L_{VPP} = g_{VPP}\, V^\mu P \overleftrightarrow{\partial_\mu} P \qquad \text{and} \qquad L_{VVP} = g_{VVP}\, \epsilon_{\mu\nu\alpha\beta}\, \partial^\mu V^\nu \partial^\alpha V^\beta P. \tag{1}$$

Let two hadrons, call them a and b, annihilate and form an intermediate state V—a vector meson in our study. Vector-meson dominance suggests that the neutral component of the hadronic vector field couples directly to the photon[4]

$$L_{VA} = \left(\frac{em_V^2}{g_V}\right) V_\mu^0 A^\mu \tag{2}$$

where V is the resonant vector field and A is the electromagnetic field. A diagram for $a+b \to V \to \gamma^* \to e^+e^-$ differs from the analogous process of purely electromagnetic exchange due to the presence of the hadronic resonance. Since its effect is a function of invariant mass alone, the hadronic dependence factorizes from the rest of the diagram as a form factor times a pointlike electromagnetic process. There appears the ratio g_{Vab}/g_V squared in the absolute square of the scattering amplitude.

We appeal to the time-reversed hadron production processes in order to fix the ratio of coupling constants. First for $e^+e^- \to \rho\pi$, the cross section is computed to be

$$\sigma_{e^+e^-\to\pi\rho}(M) = \frac{e^4|\boldsymbol{p}|^3\,|F_{\pi\rho}(M)|^2}{12\pi M^3} \tag{3}$$

where

$$m_\phi = \sqrt{\boldsymbol{p}^2 + m_\pi^2} + \sqrt{\boldsymbol{p}^2 + m_\rho^2}, \quad \text{and} \quad F_{\pi\rho}(M) = \sum_V \left(\frac{g_{V\pi\rho}}{g_V}\right) \frac{e^{i\varphi_V} m_V^2}{m_V^2 - M^2 - i m_V \Gamma_V}, \tag{4}$$

with the sum running over the three vectors $\phi(1020), \omega(1390)$ and $\omega(1600)$. Comparison with experiment constrains the ratios of coupling constants as well as the phase angles and is shown in Fig. 1a. Numerical details can be found in Ref. [5]. Similar analyses lead to an expression for $\sigma(e^+e^- \to K^0_S K^\pm \pi^\mp)$. The couplings are adjusted to obtain the agreement with experiment shown in Fig. 1b.

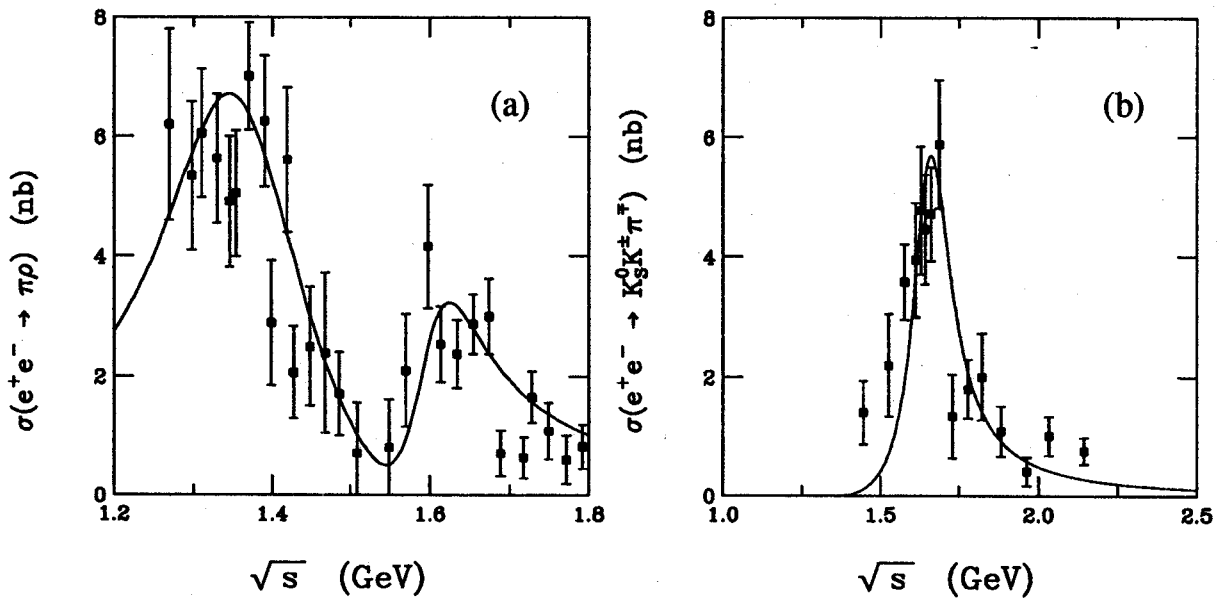

Fig. 1: Cross section for $e^+e^- \to \pi\rho$ as computed within the model described in the text as compared with experimental data from Ref. [6,7] (a), and cross section for $e^+e^- \to K^0_S K^\pm \pi^\mp$ as compared with experimental data from Ref. [8].

Under the assumption of thermalization the differential rate for a hadronic scattering which produces an e^+e^- pair of invariant mass M can be written as

$$\frac{dR}{dM^2} = \mathcal{N} \int \frac{d^3p_a}{2E_a(2\pi)^3} \frac{d^3p_b}{2E_b(2\pi)^3} \frac{d^3p_+}{2E_+(2\pi)^3} \frac{d^3p_-}{2E_-(2\pi)^3} f(E_a) f(E_b)$$

$$\times (2\pi)^4 |\mathcal{M}|^2 \delta^4(p_a + p_b - p_+ - p_-) \delta\left(M^2 - (p_+ + p_-)^2\right) \qquad (5)$$

where f is the Bose-Einstein distribution and $\mathcal{N}$ is an overall degeneracy factor. The absolute square of the scattering amplitude for $\pi\rho \to e^+e^-$ initial spin averaged and final spin summed is

$$|\mathcal{M}|^2 = \frac{4e^4}{3} \frac{|F_{\pi\rho}(M)|^2}{M^4} \epsilon_{\mu\nu\alpha\beta} \epsilon_{\kappa\lambda\sigma\tau} q^\mu q^\kappa p_\rho^\alpha p_\rho^\sigma \left(-g^{\beta\tau} + p_\rho^\beta p_\rho^\tau / m_\rho^2\right) \left[p_+^\nu p_-^\lambda + p_-^\nu p_+^\lambda - g^{\nu\lambda}(p_+ \cdot p_-)\right], \qquad (6)$$

where $q^\mu = p_+^\mu + p_-^\mu$ so that $q^2 = M^2$ and finally, where the form factor is given by Eq. (4). Making the replacements $m_\rho \to m_{K^*}$ and $p_\rho \to p_{K^*}$ and using a form factor essentially like Eq. (4) but modified to include only $\phi(1680)$ gives the squared amplitude for the process $\bar{K}K^* + \text{c.c.} \to e^+e^-$.

After contracting the indices in Eq. (6) and performing the thermally weighted phase space integral in Eq. (5), we reach the results at 150 MeV temperature presented in Fig. 2. For comparison purposes we also include the results for $\pi^+\pi^-$ annihilation [9] and for πa_1 reactions Ref. [10] which were concluded to be dominant for masses above m_ϕ. The importance of the excitations of $\omega(1390)$ and $\phi(1680)$ are immediate: they are visible above the tail of the $\pi^+\pi^-$ annihilation and even above the πa_1 results.

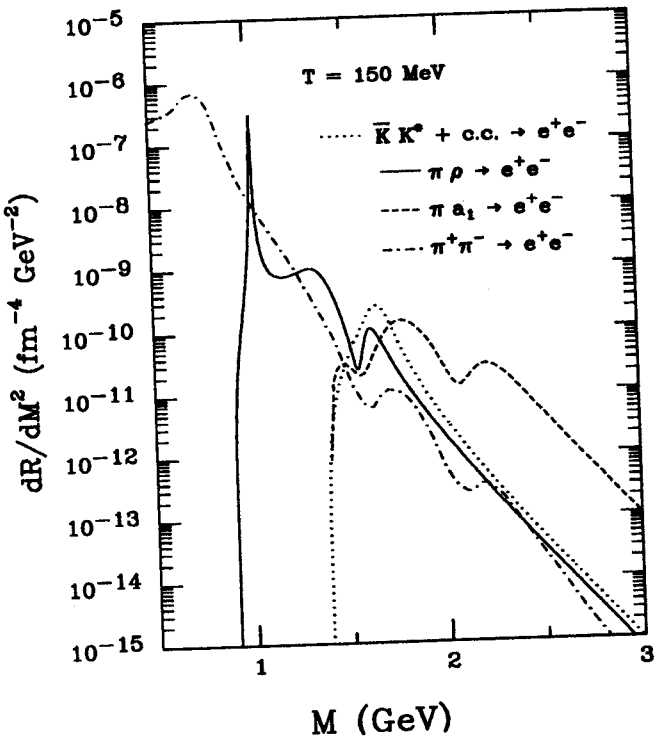

Fig. 2: Thermal production rate at $T = 150$ MeV from $\pi\rho$ (solid curve) processes, $\bar{K}K^*$+c.c. (dotted curve), $\pi^+\pi^-$ annihilation from Ref. [9] (dot-dash curve) and finally, πa_1 process as calculated in Ref. [10] (dashed curve).

In our study we have constructed effective form factors $|F_{\pi\rho}(M)|^2$ and $|F_{KK^*}(M)|^2$ in the mass range 1–2.5 GeV. After doing so, we have compared each elementary process with known data before using them in a thermal calculation on the extended system of interacting hadrons. Higher excitations of the ω and ϕ, namely $\omega(1390)$ and $\phi(1680)$, were found to be visible in the mass distribution of the dilepton production rate above the hadronic production mechanisms previously considered. This clearly suggests that in order to improve knowledge of dielectron production rates from hot hadronic matter, at least for dielectron masses ranging from m_ϕ to $m_{J/\psi}$, form factors for hadrons other than just the pion must be considered.

a. Physics Department, McGill University, Montréal, QC, H3A 2T8, Canada.

References

1. K. Haglin and C. Gale, preprint MSUCL-934 and McGill University report McGill/94-44.
2. K. Haglin and S. Pratt, Phys. Lett. B 328, 255 (1994).
3. U.-G. Meissner, Phys. Rep. 161, 213 (1988).
4. J.J. Sakurai, Ann. Phys. (N.Y.) 11, 1 (1960).
5. K.L. Haglin and C. Gale, Nucl. Phys. B421, 613 (1994).
6. V.M. Aulchenko *et al.* Novosibirsk Preprint 86–106 (1986); A. Donnachie and A.B. Clegg, Z. Phys. C 42, 663 (1989).
7. R. Baldini–Ferroli in Proc. Had. Phys. at Intermediate Energy, T. Bressani, B. Menetti, and G. Pauli (eds.) Amsterdam, New York, Elsevier (1987); A. Donnachie and A.B. Clegg, Z. Phys. C 42, 663 (1989).
8. F. Mane, *et al.*, Phys. Lett. B 112, 179 (1982).
9. C. Gale and P. Lichard, Phys. Rev. D 49, 3338 (1994).
10. C. Song, C.M. Ko and C. Gale, Phys. Rev. D 50, R1827 (1994).

COLLISION RATES FOR ρ-, ω-, AND ϕ-MESONS AT NONZERO TEMPERATURE

Kevin P glin

Vector meson behaviour at nonzero temperature is particularly important for systems created in ultra-relativistic heavy-ion collisions. Details of their creation, propagation and decay greatly affect the overall many-body dynamics of the collisions and consequently the observed particle spectra. In this finite temperature medium they will scatter with other hadrons in their approach to equilibrium and thereafter. These dynamics induce broadening to the already unstable vector mesons which is calculated in the framework of relativistic kinetic theory. A rather complete set of low-lying mesons provide reaction partners whose interactions are modeled using effective Lagrangians. Collision rates for ρ and ω are found to be $\sim$ 100 MeV at T=200 MeV while the rate for ϕ is $\sim$ 25 MeV[1].

One might model the late stage of the collision as a thermal ensemble of low-lying hadrons: pions, kaons, ρ and $K^*(892)$ mesons as well as some heavier axial-vectors $a_1(1260)$, $b_1(1235)$ and $K_1(1270)$. The ϕ meson resides here also and like the others will be assumed to be thermalized. These particles are quantified as fields which interact according to the following Lagrangians[2,3]

$$\begin{aligned} L_{VPP} &= g_{VPP}\, V^\mu P \overleftrightarrow{\partial_\mu} P \\ L_{VVP} &= g_{VVP}\, \epsilon_{\mu\nu\alpha\beta}\, \partial^\mu V^\nu \partial^\alpha V^\beta P \\ L_{AVP} &= g_{AVP}\, A_{\mu\nu} V^{\mu\nu} P \end{aligned} \tag{1}$$

where the field strength tensors are $A_{\mu\nu} = \partial_\mu A_\nu - \partial_\nu A_\mu$ and similarly for $V^{\mu\nu}$. In the above expressions A, P and V refer to axial-vector, pseudoscalar and vector meson fields.

Since hadronic cross sections tend to be dominated by resonances, one naturally looks to $\rho\pi$ scattering through $a_1(1260)$, ρK scattering through $K_1(1270)$, $\omega\pi$ scattering through $b_1(1235)$ and to strange-particle possibilities for the ϕ. Although it can form $K_1(1770)$ and $K_4(2045)$ when scattering with kaons and K^* s, the branching ratios are very small leaving them inconsequential. There are also resonance possibilities in the non-strange sector. Scattering with pions is probable while forming $b_1(1235)$ or even $\rho(1450)$ mesons. The branching ratios are not firmly established, but tentative upper limits of 1.5 and 1 percent have been quoted[4]. Then in the t channel there are several seemingly equally important possible configurations since all three vector mesons can scatter with pions, kaons and a host of others.

In t-channel reactions between particles 1 and V where particle E is exchanged and where $m_1 + m_E < m_V$, phase space allows the squared four-momentum of the exchanged particles to access timelike values and even become equal to m_E^2. If t is identically equal to m_E^2 then one has a true on-shell decay instead of scattering. This must be interpreted carefully so as to avoid double counting. An imaginary part is introduced into the propagators to account for the effects of the matter, i.e. $1/(t - m_E^2 - im_E\Gamma_E)$. Hadrons necessitate the use of form factors since they are composite objects and have finite extent which can be seen when probed with higher and higher momentum transfers. A suppression of this region is physically imperative. The standard way to accomplish this is to insert a monopole form factor. The particular reaction $\rho + \pi \to \rho + \pi$ must be treated carefully since the monopole must be "renormalized". For details see Ref.[1].

Coupling constants naturally appear in the scattering amplitudes. They are adjusted in order to obtain the observed partial decay rates. Relevant rates for general decays are computed starting from the

interactions in Eq. (1) to be

$$\Gamma_{V\to PP'} = \frac{g_{VPP'}^2}{6\pi}\left(\frac{|p|^3}{m_V^2}\right), \qquad \Gamma_{V\to PV'} = \frac{g_{VPV'}^2}{12\pi}|p|^3,$$

$$\Gamma_{A\to VP} = \frac{g_{AVP}^2}{6\pi}|p|\left(\frac{\left(m_A^2+m_V^2-m_P^2\right)^2}{2m_A^2}+m_V^2\right), \tag{2}$$

where p is the center-of-mass momentum of the decay products. From here one can get all the necessary coupling constants.

Timelike and intermediately propagating pions or kaons acquire imaginary parts due to the presence of the matter which are approximated by computing the dominant scattering rates. For instance, pions will scatter with other pions—a process dominated by the ρ resonance. They will also scatter with kaons to form $K^*(892)$ resonances. The rate at which each of these happens is

$$\Gamma_b^{\rm coll}(E,T) = \int ds\,\frac{d^3p_\pi}{(2\pi)^3} f_\pi \sigma_{b\pi}(s) v_{rel}\,\delta\left(s-(p_b+p_\pi)^2\right), \tag{3}$$

where f is the Bose-Einstein distribution function and

$$v_{rel} = \frac{\sqrt{(p_b\cdot p_\pi)^2 - 4m_b^2m_\pi^2}}{E_bE_\pi} \quad \text{and} \quad \sigma_{b\pi}(\sqrt{s}) = (2J_{\rm res}+1)\,\frac{\pi}{k^2}\,\frac{\Gamma_{{\rm res}\to b\pi}^2}{(\sqrt{s}-m_{\rm res})^2+\Gamma_{\rm res}^2/4} \tag{4}$$

is used with k being the center-of-mass momentum, "res" refers to the resonance through which it proceeds and b refers generally to pions or kaons. The width is a function of the three-momentum separately and is therefore frame-dependent but determined by the hadron gas. Depending on the temperature and on the pion or kaon momenta, widths vary from 20 to 200 MeV. Results similar to these were recently obtained for the momentum dependent scattering rate of ω mesons at finite temperature using this prescription[5].

For a general (bosonic) reaction involving the vector V and having the form $V+a\to 1+2$, the kinetic theory expression for an average scattering rate is

$$\bar{\Gamma}_V^{\rm coll} = \frac{1}{n_V} d_V d_a \int d^3\bar{p}_V d^3\bar{p}_a d^3\bar{p}_1 d^3\bar{p}_2 |\bar{\mathcal{M}}|^2 (2\pi)^4\delta^4(p_V+p_a-p_1-p_2)$$

$$\times f_V f_a (1+f_1)(1+f_2) \tag{5}$$

where $d^3\bar{p}_V = d^3p_V/2E_V(2\pi)^3$ and similarly for the others, where the bar over the squared scattering amplitude indicates that an initial spin average and final spin sum must been done, where f is again the Bose-Einstein distribution, the d s are degeneracy factors, and n_V is the number density of V's.

Many results for partial thermal widths are obtained for all three light vector mesons. For instance, ρ and ω collisional widths are found to be of the order 100 MeV at high temperatures. The ϕ is less reactive and has a smaller rate since there isn't a strong $\phi+x$ resonance where x might be a pion,

kaon, K^* etc. Thus, many channels must be considered. For details on the one and a half dozen channels included the reader is urged to consult Ref.[1]. The sum of all contributions to the ϕ's thermal width is shown in Fig. 1a. From here it is trivial to produce a mean free path which is shown in Fig. 1b along with the results for ρ and ω.

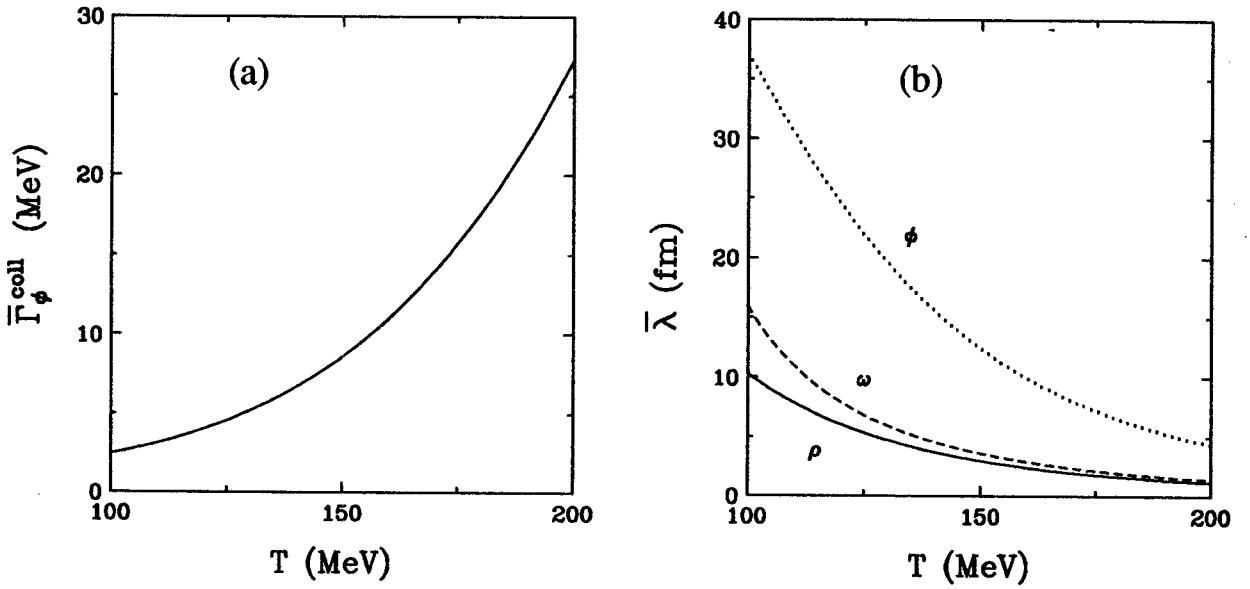

Fig. 1: Collision rate for the ϕ as a function of temperature (a), and mean free paths for ρ, ω and ϕ in (b).

A summary of the results goes as follows. At low temperatures, by which 100 MeV or so is meant, the collision rates for all three were quite small $\sim$ 10, 6, and 2 MeV for ρ, ω and ϕ. Results for each of them rises monotonically as the number densities of pions and kaons increase. As temperatures rise above the pion mass, the number densities of species other than pions and kaons become large enough so that collisions with the ϕ are more frequent. Scattering of ϕ mesons with ρ and K^* mesons becomes significant around 150 MeV temperature while at high temperatures several processes contribute nearly equally resulting in a total rate of 27.2 MeV at $T = 200$ MeV. At this extreme, the mean free path of ϕ mesons is 4.4 fm! These time and distance scales could have noticeable consequences on some observables at least for ω and ϕ-related ones. A place to look for possible observable modification is in dilepton invariant mass spectra.

References

1. K. Haglin, Nucl. Phys. A 584 719 (1995).
2. U.-G. Meissner, Phys. Rep. 161, 213 (1988).
3. G. Jansssen, K. Holinde and J. Speth, Phys. Rev. C 49, 2763 (1994).
4. Particle Data Group, K. Hikasa *et al.*, Phys. Rev. D 45, p. II.6–II.11 (1992).
5. K. Haglin, Phys. Rev. C 50, 1688 (1994).